https://doi.org/10.1016/j.ijhydene.2019.11.131

Atomistic simulation study of the grain-size effect on hydrogen embrittlement of nanograined Fe

Xiao-Ye Zhou[a1], *Xu-Sheng Yang*[b1], *Ji-Hua Zhu*[a]*, *Feng Xing*[a]

[a] Guangdong Province Key Laboratory of Durability for Marine Civil Engineering, School of Civil Engineering, Shenzhen University, Shenzhen, Guangdong 518060, PR China.

[b] Advanced Manufacturing Technology Research Center, Department of Industrial and Systems Engineering, The Hong Kong Polytechnic University, Hung Hom, Kowloon, Hong Kong, China

Abstract

Although hydrogen-induced fracture at grain boundaries has been widely studied and several mechanisms have been proposed, few studies of nanograined materials have been conducted, especially for grain sizes below the critical size for the inverse Hall-Petch relation. In this research work, molecular dynamics (MD) simulations are performed to investigate the hydrogen segregation and hydrogen embrittlement mechanism in polycrystalline Fe models. When the same concentration of H atoms is added, the H segregation ratio in the model with the smallest grain size is the highest observed herein, showing the high hydrogen trapping ability of small-grain Fe, while the H concentration at the grain boundaries (GBs) is, on the contrary, the lowest. Uniaxial tensile test simulations demonstrate that as the grain size decreases, the models show an increased resistance to hydrogen embrittlement, and for small-grain models (d <10 nm), the GB-related deformation modes dominate the plastic deformation, where the segregated H mainly influences the toughness by inhibiting GB-related processes.

Introduction

* Corresponding author: zhujh@szu.edu.cn

[1] These authors contributed equally to this work.

Grain refinement is a commonly used method for improving mechanical properties of metals, such as yield strength and hardness, because grain boundaries (GBs) can act as obstacles to dislocation movement. The strength increase associated with reduced grain size is usually described in terms of the well-known Hall-Petch relation. With advances in manufacturing technology, grain refinement to the nanoscale regime can be achieved. Typical fabrication methods include severe plastic deformation[1-4], inert gas condensation[5] or electrochemical deposition[6]. With proper parameter control, grains could be as fine as ~10 nm after treatment[7], which is much smaller than grains produced by traditional mechanical treatments. For nanograined metals, GBs often play a major role in the plastic deformation process. GB-related deformation modes that have been observed in nanograined metals include dislocation nucleation from GBs[8], deformation twins[9-11], grain rotation[12], and GB sliding and migration[12-13]. GB-related deformation usually has an inverse influence on the strengthening effect of GBs, causing a breakdown of the Hall-Petch relation. It has also been suggested that a critical grain size of approximately 10-15 nm[13] exists below which the Hall-Petch relation is inversed, and a continued reduction in the grain size would soften, rather than strengthen, the metal.

Hydrogen embrittlement (HE), also known as 'hydrogen-induced cracking', is a phenomenon in which the mechanical properties of metals, especially the plasticity and durability, deteriorate significantly due to the atomic hydrogen present in the metals[14]. Hydrogen atoms can be absorbed into metals during the manufacturing process or from various service environments, such as those that include hydrogen gas, a corrosive liquid or cathodic protection[15-16]. Atomic hydrogen can segregate to crystal defects, such as vacancies[17-18], dislocation cores[19], GBs[20-21] and precipitates[22-23]. A substantial amount of research has shown that for metals charged with relatively high concentrations of hydrogen, intergranular, rather than intragranular, fracture usually happens, indicating that GBs play an important role during the HE of polycrystalline metals[24-27]. To explain the occurrence of intergranular fracture, the hydrogen-enhanced decohesion (HEDE) mechanism[28] was proposed. Theoretical calculations have also suggested the ability of hydrogen atoms to

reduce GB cohesive strength[29-32]. However, HEDE alone could not fully explain experimental observations, such as quasi-cleavage fractures and dislocation pile-up that have been found beneath the fracture surface of intergranular fracture samples. A hydrogen-enhanced-plasticity-mediated decohesion mechanism[33] was then proposed to complement HEDE in explaining GB-related HE. This mechanism combines HEDE with the hydrogen-enhanced local plasticity (HELP) modes, suggesting that GBs are not only weakened by hydrogen, but that the dislocations piled up near the GBs also contribute to the intergranular fracture.

Now that GBs play such an important role in HE, increasing the GB density by grain refinement should have an effect on the HE properties of polycrystalline metals. In fact, it has been shown that grain refinement can improve HE resistance. Mechanical treatments, such as high-pressure torsion[34-35], multi-pass rolling[36], and dynamic plastic deformation[37], in addition to heat treatments, like intercritical annealing[38] have been performed to refine the grain size in steels, and the treated steels show improved resistance to HE. Mechanisms for the enhanced HE resistance were proposed, including a decreased H concentration value at the GBs[36, 39], a decreased number of deformation twins[38] and an increased probability of crack initiation[35] when the grain size decreases. However, due to the difficulty of observing the hydrogen distribution and measuring the local hydrogen content experimentally, in addition to the complicated microstructure of the studied steels, the proposed mechanisms cannot clearly elucidate the role that GBs play in enhancing HE resistance. Besides, the grain refinement methods used in those studies only refine grains to the micrometer scale. As stated previously, when using an advanced manufacturing technique, it is possible to fabricate nanograined metals with a grain size of approximately 10 nm, which is even smaller than the critical grain size for the inverse Hall-Petch effect. In nanograined metals, GB-related deformation modes play a major role in the deformation process, while in coarse-grain metals, dislocation nucleation and motion in grain interiors are the main deformation modes. When H atoms are involved, they segregate to GBs so that GB-related deformation modes are highly affected. Therefore, the HE mechanism in nanograined materials should be different from that in their

coarse-grain counterparts due to the increased importance of the interaction of H with the GBs in nanograined materials.

Atomistic simulation is a widely adopted tool for studying the HE mechanism[40-45] and deformation processes of nanograined materials[46-51]. While it is usually difficult to directly observe distributions of H atoms, the interaction of H atoms with crystal defects, or the GB and dislocation motions in nanograined materials during deformation through experimental methods, atomistic simulations can overcome such limitations. In this work, we performed molecular dynamics (MD) simulations to investigate the effect of grain size on the HE mechanism in nanograined body-centered cubic (bcc) Fe. We selected bcc Fe as the research object because Fe is the main component in steel, which is an important structural material. Although it is commonly recognized that high-strength steels are highly susceptible to HE, pure Fe can also be embrittled when it is charged with a high concentration of hydrogen[24]. Nanograined models with the same GB arrangement but different grain sizes were built to simulate different levels of grain refinement. Hydrogen segregation was simulated by inserting H atoms followed by high-temperature annealing. Tensile tests were simulated to investigate the influence of hydrogen on the mechanical properties of the simulated models. The H-induced fractures in the models with different grain sizes are compared to reveal the grain-size effect on HE mechanism. It is found that in the large-grain models, dislocation activities are the main deformation modes, and the HE mechanism involves the interaction of dislocations, GBs and H atoms, as described by the 'hydrogen-enhanced-plasticity-mediated decohesion' mechanism[29, 33]; in the small-grain models, GB-related deformation dominated the plastic deformation. The segregated H was found to mainly influence the toughness of the models by inhibiting GB-related deformation.

Simulation methodology

Nanograined Fe models were built by using two-dimensional (2-D) Voronoi tessellation to separate cubic cells into polyhedrons. Each polyhedron was filled with bcc Fe atoms aligned along a random orientation. Atoms that overlapped (interatomic distance < 0.14 nm) were deleted. To simulate nanograined Fe with various grain sizes, we modeled cubic cells

with 8 different in-plane (x-y plane) dimensions. The out-of-plane dimension (z direction) was the same for all models and was 10 nm. The 8 models had the same grain arrangement and orientation. The only difference was the grain size. The 8 nanograined models had average in-plane grain diameters of 6 nm, 7 nm, 8 nm, 9 nm, 10 nm, 12 nm, 18 nm, and 24 nm, and are denoted hereafter as NG_d, with d being the grain size. Periodic boundary conditions were imposed along all directions. The interatomic interaction was described by an embedded-atom method (EAM) potential developed by Ramasubramaniam et al. This EAM potential was developed for hydrogen in bcc Fe based on density functional theory. It has been widely used to study the HE in Fe with MD simulations[29, 44, 52-54]. After the construction of the nanograined models, MD simulations of the heating and cooling processes were performed using the Large-scale Atomic/Molecular Massively Parallel Simulator (LAMMPS) software[55] to obtain equilibrium atomic structures. The models were first heated to 700 K and maintained for 1 ns. They were then cooled to 300 K in 0.3 ns. The annealing temperature and time were selected to avoid grain growth. After annealing, the equilibrated structures of the models were obtained and plotted in Fig. 1. Atomic structure visualization was achieved using the Open Visualization Tool (OVITO)[56] with crystal structures calculated by common neighbor analysis[57]. To visualize the dislocation distribution in the annealed models, dislocation analysis was performed using the dislocation extraction algorithm (DXA) tool in the OVITO. The dislocation lines found by the DXA were colored according to their types.

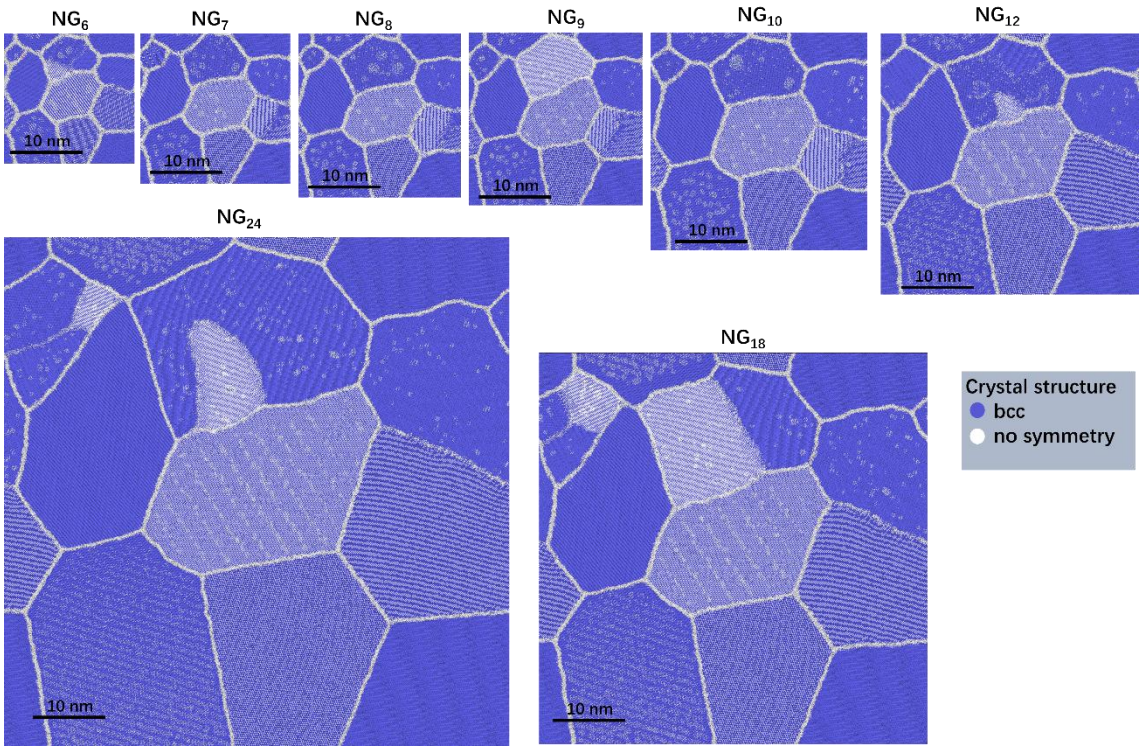

Fig. 1. Atomic structures of nanocrystalline Fe models with different grain sizes. The bcc atoms are colored blue, while atoms with no symmetry are white.

To reveal the effect of grain refinement on the HE of nanograined Fe, we first simulated H segregation in 4 models with discrete grain sizes of 6 nm (NG_6), 12 nm (NG_{12}), 18 nm (NG_{18}) and 24 nm (NG_{24}). H atoms were added to the interstitial sites of the annealed nanograined models. H concentrations for the models were kept the same. Three levels of total H concentration were adopted to represent low, medium high, and very high H concentrations. The H atomic percent for the 3 levels of H concentration were 0.4% (denoted as H_1 hereafter), 1.5% (H_2) and 3% (H_3). After the insertion of the H atoms, the models were again heated to 700 K and maintained for 1 ns to allow the H atoms to fully segregate to defect sites. They were then cooled to 300 K in 0.3 ns. For NG_{24}, because the grain size is larger than that of the other models and H atoms would need an extended period of time to fully segregate to the GBs, a prolonged annealing time of 1.5 ns was used.

Uniaxial tensile tests were simulated by straining the models along the y direction at 300 K while keeping the x and z directions stress free. The strain rate in all tensile simulations was kept at 5×10^8/s, which is very high compared with real experiments. We first conducted

tensile tests on pure Fe models, and then tensile tests were performed on models with H atoms inserted. Under the current high strain rate at a room temperature of 300 K, H could not diffuse toward high stress regions and accumulate at defect sites that were generated during elongation. Therefore, the interaction of H with the generated defects cannot be observed in the present simulations. However, the interactions of the GB-segregated H with the GBs and the dislocations and twins that were emitted from the GBs could be observed, which is the focus of this study.

Results and discussion

1. Tensile simulations of nanograined Fe models without H

Fig. 2 a-c plot the deformation snapshots of the models with several typical grain sizes of 24 nm, 10 nm, and 6 nm, from which we can see the grain size-dependent deformation mechanisms in the nanograined materials. In NG_{24}, dislocation nucleation and movement inside the grains are found in several locations, as denoted in Fig. 2a. Dislocation nucleation at the GBs is also found. Dislocation pile-up at the GBs can be observed at several locations, indicating that the grain size of 24 nm is large enough for dislocation pile-up. Deformation twins are only observed in a few grains and occur later than dislocation nucleation and movement, indicating that the partial dislocations that generate twins play a less important role than full dislocations in the deformation process of the NG_{24} model.

In NG_{10} (Fig. 2b), deformation twins are observed more often than in NG_{24}. GB migration, grain growth and rotation can also be observed. Judging by the changes in the grain shapes and GB structures, we can see that GB-related intergranular deformation modes also play an important role during the deformation of NG_{10}. The deformation mechanism of the deformation twin was described by Zhang et al. in their MD simulation work on the deformation process of nanograined bcc Mo[51, 58] with grain sizes up to 34 nm. Our simulation results also confirmed the important role of deformation twins in nanograined Fe. After twinning, grain rotation and grain growth happen. This grain rotation and growth induced by deformation twinning were reported by Lue et al.[11] in their study of ~19 nm

gold nanograined films and were found to be an important deformation mechanism in nanograined materials.

In model NG_6 (Fig. 2c), which is the model with the smallest grain size in our simulations, most of the grains change their shapes, and most GBs move after deformation. Therefore, we suggest that GB-related deformation is the main deformation mechanism during the plastic deformation of NG_6. A deformation twin that nucleates at the GBs can be observed during the deformation of NG_6, and the twin finally induces GB fracture at the GB triple junction. Dislocations that nucleate and vanish at the GBs are observed during deformation. The passage of dislocations alters the orientation of the atoms in that grain. GB sliding and migration are also observed, and they subsequently induce the growth or fragmentation of grains (grain A in Fig. 2c). No dislocation nucleation at the grain interior or dislocation pile-up can be observed. Although the deformation was not measured quantitatively, we can roughly see that the dominant GB-related intergranular deformation mechanism in NG_6 not only includes GB sliding, migration, grain rotation and growth but also includes deformation twins and dislocations that nucleate at the GBs.

By comparing the deformation processes of NG_{24}, NG_{10}, and NG_6, we can see a transition in the deformation modes from intragranular to intergranular. A large-grain model that has grain sizes above the critical size for the inverse Hall-Petch relation deforms mainly by intragranular deformation, where full dislocation nucleation from the grain interior, dislocation propagation and pile-up are frequently observed. However, in small-grain models, the deformation modes are mainly GB-related. Table 1 lists the ratio of GB atoms versus total atoms. In NG_{24}, only 2.25% of the atoms are GB atoms, while that number is 8.5% for NG_6. The higher portion of GB atoms and higher GB density for NG_6 facilitate the GB-related deformation modes, such as GB sliding, GB migration, grain rotation and grain growth. Deformation twins and dislocations that nucleate at GBs can also be deemed GB-related deformation; hence, they are also facilitated in small-grain models. The difference in the deformation modes of nanograined Fe suggests that the HE mechanism should be grain size dependent, which is evaluated in the following discussions.

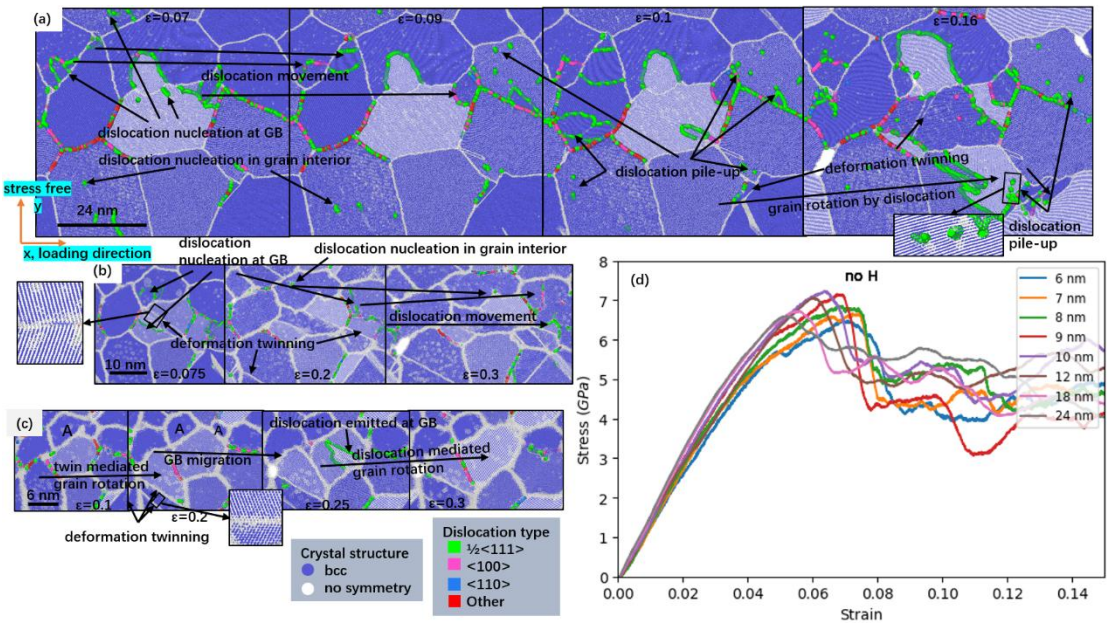

Fig. 2. (a)-(c) The atomic configurations of NG_{24}, NG_{10}, and NG_6 during deformation. GB migration, grain rotation, grain growth, dislocation nucleation, dislocation movement, dislocation pile-up, and deformation twins are indicated by arrows. Dislocation lines are colored by their types. (d) The stress-strain curves of the 8 nanograined models with different grain sizes ranging from 6 nm to 24 nm.

The stress-strain curves of the 8 nanograined models with different grain sizes are plotted in Fig. 2d. A decrease in the slopes of the initial stress-strain relations as the grain size decreases is observed. This phenomenon can be explained by the increasing GB fraction as the grain size decreases, which has been discussed by Shimokawa et al.[49] They suggested that as the fraction of atoms at the GBs increases with a decrease in the grain size, GB-related intergranular deformation becomes easier than intragranular deformation. The intergranular deformation occurs prior to intragranular deformation, resulting in a decreased slope in the initial stress-strain curves. The peak stress, on the other hand, first increases as grain size decreases but then decreases, following an inverse Hall-Petch relation where the critical grain size is approximately 10 nm.

3. Hydrogen segregation in nanograined Fe models

To investigate the grain-size effect on the HE mechanism, we first added H atoms to the

models and let the H atoms fully segregate to the GBs. The distribution of the H atoms in the 4 models after annealing is shown in Fig. 3, from which we can see that the annealing process did not change the grain arrangement and the GBs remained at their equilibrium positions. Most of the H atoms segregate to the GBs and other defect sites, such as dislocation cores and vacancies, while some are located at normal interstitial sites.

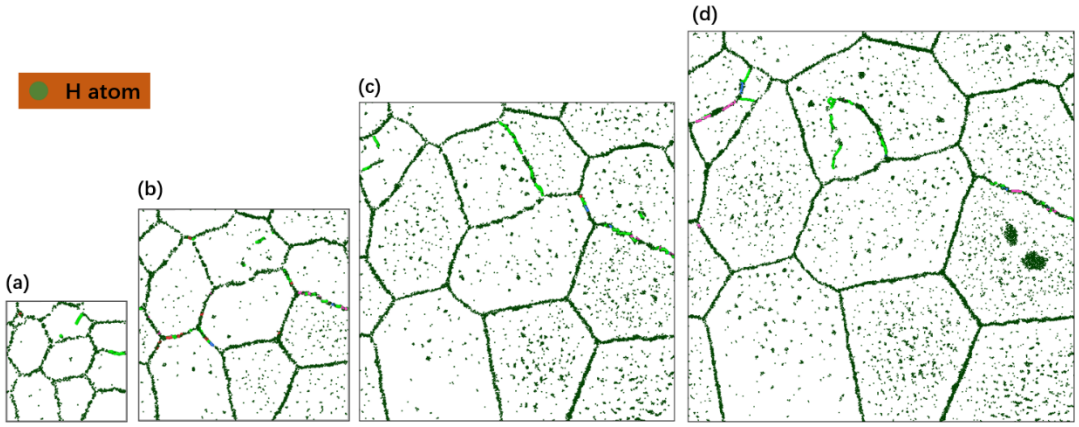

Fig. 3. H distribution in (a) NG_6, (b) NG_{12}, (c) NG_{28}, and (d) NG_{24}. The H concentration in this figure is 3% (H_3). Dislocation lines are colored by their types, as in Fig. 2.

To characterize the GBs in the 4 nanograined models, we first calculated the length of the GB per unit area (l-GB) and GB atom ratio (number of GB atoms against total number of atoms, GB atom%), which are shown in Table 1. The GB free volume (FV), which is the excess volume due to the existence of GBs, is another important characteristic of GBs. Here, we calculated the FV in the 4 nanograined models by:

$$FV = \left(V_{poly} - V_{bulk}\right)/V_{poly} \quad (1)$$

where V_{poly} is the volume of the model after annealing and V_{bulk} corresponds to the volume of the bulk bcc Fe with the same number of atoms as the nanograined model. The calculated FV values are shown in Table 1, which shows that GB length, FV, and GB atom ratio have a positive correlation with each other.

After the H segregation simulations of the 4 nanograined models were completed, H atoms that segregated to the GBs were counted, and the segregation ratios were calculated, which are listed in Table 1. For the 4 nanograined models, the segregation ratio (Seg-H_1, H_2, H_3) is almost independent of the H concentration and decreases as the GB density

(represented by *l*-GB), GB atom ratio and FV decrease. In an equilibrium state, the segregation ratio should only depend on the number of segregation sites and the segregation energy at that site; therefore, for the same model, the H segregation ratio should be the same. The variance in the segregation ratio originates from defect sites other than GBs in the models that also trap H atoms. However, the defect sites, like dislocation cores and vacancies, are much lower in number than the number of GB trapping sites; therefore, they saturate quickly with the rest of the H atoms segregate to the GBs. This explains the increased segregation ratio as the H concentration increases. Upon comparing the segregation ratio of models with different grain sizes, we can see that as the grain size decreases, the segregation ratio increases, which means that small-grain models have a higher H trapping ability than the large-grain models.

The H concentration at the GBs (H_{GB}) of the 4 models with 3 levels of H concentrations are listed in the last 3 columns of Table 1. The value of H_{GB} is calculated as the number of H atoms per unit length (nm) in the GBs. By comparing the H_{GB} of the 4 nanograined models, we find that as the grain size decreases, the H_{GB} also decreases. Owing to the refined grain size, NG_6 has a much higher GB density than NG_{18} and $NG_{24;}$ thus, even though the segregation ratio of NG_6 is the highest, its H_{GB} is only half that of NG_{18} and NG_{24}, rendering it more resistant to HE than NG_{18} and NG_{24}.

Table 1. GB length (*l*-GB), FV, GB atom ratio (GB atom%), and H segregation ratio at the GBs at 3 H concentration levels (Seg-H_1, H_2, H_3), and the H concentration at GBs at 3 H concentration levels (H_{GB}- H_1, H_2, H_3) in NG_{24}, NG_{18}, NG_{12}, and NG_6.

Grain size	***l*-GB (Å/nm^2)**	**FV (%)**	**GB atom%**	**Seg-H_1**	**Seg-H_2**	**Seg-H_3**	**H_{GB}-H_1**	**H_{GB}-H_2**	**H_{GB}-H_3**
24 nm	0.063	0.32	2.25%	0.484	0.523	0.530	76.15	301.03	659.09
18 nm	0.084	0.37	2.96%	0.536	0.554	0.588	65.15	242.76	551.16
12 nm	0.126	0.42	4.37%	0.681	0.712	0.722	54.70	211.53	457.28
6 nm	0.253	0.55	8.50%	0.844	0.863	0.898	31.17	124.31	287.25

4. Uniaxial tensile test simulations in H-segregated nanograined Fe models with different grain sizes

Uniaxial tensile test simulations were then performed on the H-segregated NG_{24}, NG_{18}, NG_{12}, and NG_6 to obtain their mechanical response under the influence of hydrogen. The maximum strain is 50%. The stress-strain curves of the models at 4 different H concentrations, which include no H, H_1, H_2, and H_3, are plotted in Fig. 4.

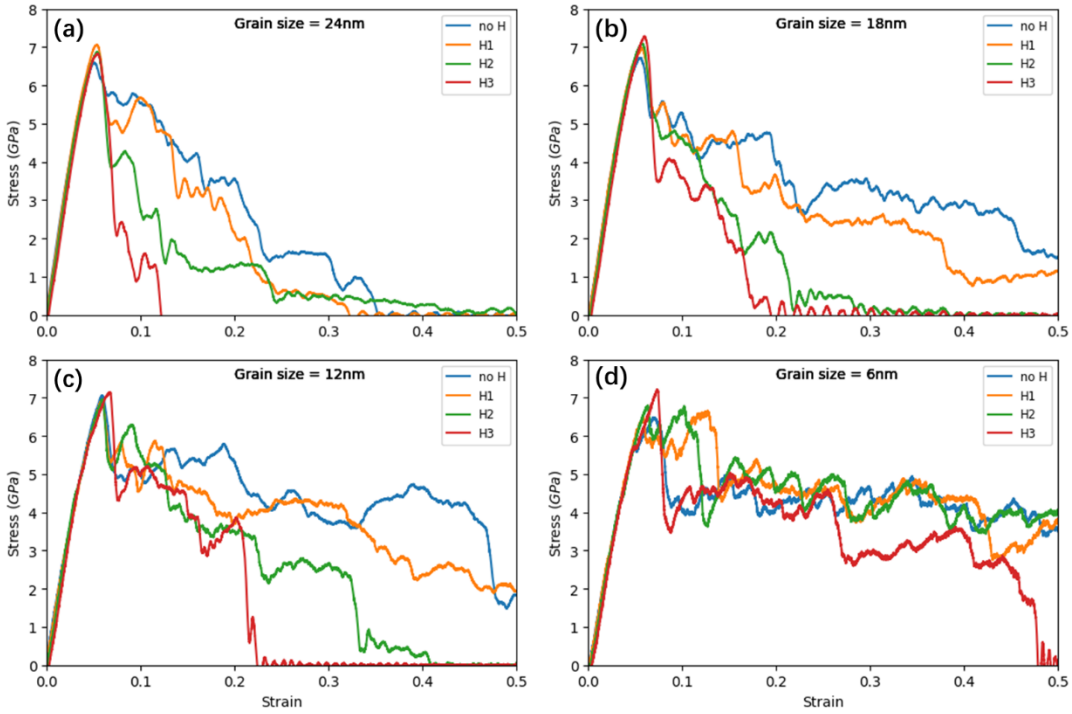

Fig. 4. Stress-strain curves from the (a) NG_{24}, (b) NG_{18}, (c) NG_{12}, and (d) NG_6 models with no hydrogen and hydrogen concentrations of H_1, H_2, and H_3.

24 nm grain model (NG_{24})

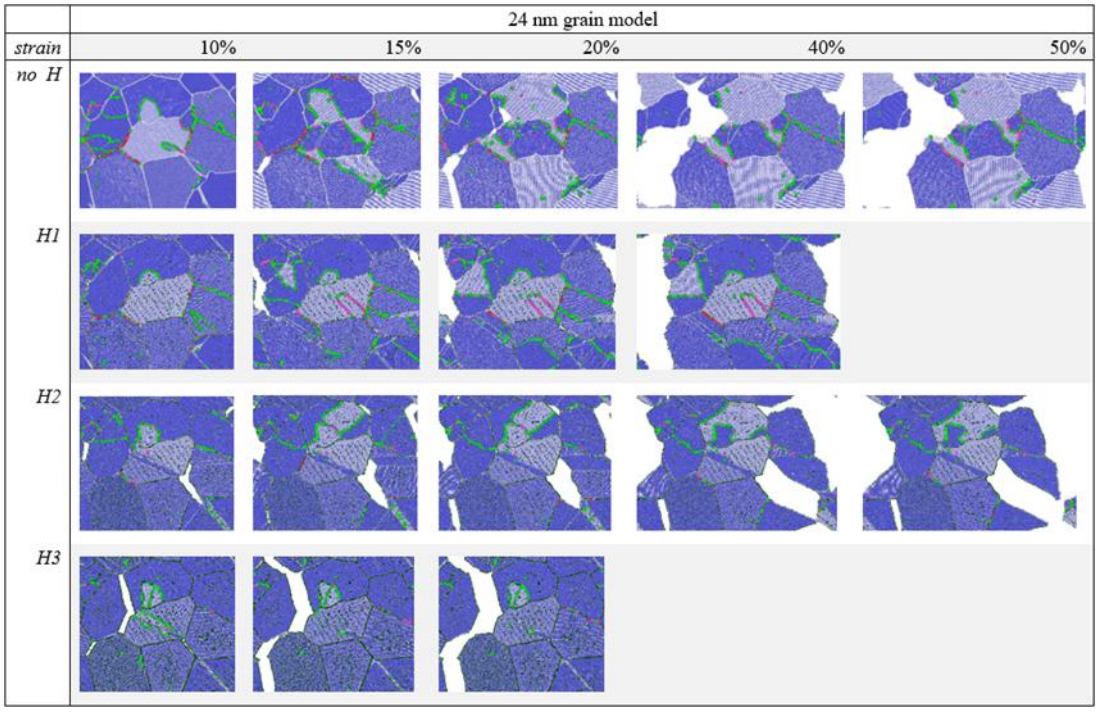

Fig. 5. The snapshots of NG_{24} without H and with H concentrations of H_1, H_2, and H_3 at 10%, 15%, 20%, 40% and 50% uniaxial strains.

The atomic configuration snapshots at 10%, 15%, 20%, 40% and 50% strain of NG_{24} during tensile simulations are plotted in Fig. 5. Fe atoms are colored according to common neighbor analysis, as in Fig. 1, and H atoms are colored dark green and are enlarged for better observation. Dislocation lines are marked and colored according to their types. The corresponding stress-strain curves are shown in Fig. 4a. As stated in the previous section, plastic deformation of NG_{24} happens mainly through dislocation activities. From Fig. 5, we can see that when a low concentration of H is added, as in the no H and H_1 cases, dislocation nucleation in the grain interior and dislocation movement can be observed, and dislocation pile-ups are found near several GBs, indicating that intragranular deformation rather than intergranular deformation is dominant for NG_{24}. From the curved fracture surface and crack tips found inside grains in the no H case, we can also see that the fracture mode is ductile rather than brittle.

As the H concentration increases, the fracture surfaces become flat. In the H_3 case, the model fractures within 20% strain, indicating a large amount of ductility loss due to H segregation at the GBs. In NG_{24}, we suppose that for the high H concentration case, the HE

mechanism is mainly the HEDE mechanism, where the cohesive strength of the GBs is greatly reduced by H segregation, and GBs fracture at relatively low strain, as seen in the stress-strain relation in Fig. 4a. For the low H concentration case, the more complicated hydrogen-enhanced- plasticity-mediated decohesion mechanism should be applied, which suggests that the HE mechanism involves the interaction of H atoms, dislocations and GBs. However, due to the timescale limitation, we cannot simulate H diffusion toward dislocation cores, which can facilitate dislocation movement and enhance local plasticity. Therefore, hydrogen-enhanced-plasticity is difficult to observe in the present MD simulation work.

18 nm grain model (NG_{18})

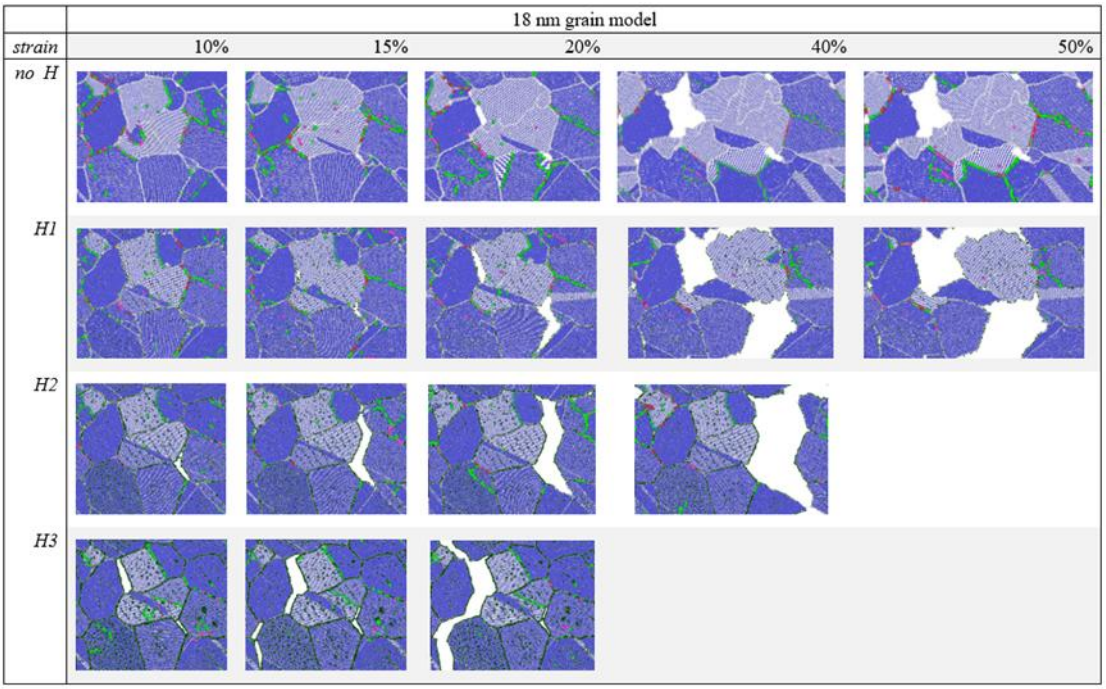

Fig. 6. The snapshots of NG_{18} without H and with H concentrations of H_1, H_2, and H_3 at 10%, 15%, 20%, 40% and 50% uniaxial strain.

The snapshots of NG_{18} during tensile simulations are plotted in Fig. 6. The corresponding stress-strain curves are shown in Fig. 4b. Similar to NG_{24}, dislocation nucleation and movement in the grain interior can be observed. For cases with low H concentrations, dislocation activities, including dislocations nucleated at the GBs and grain interiors, dominate the plastic deformation process. GB sliding, GB migration, grain rotation, grain growth and deformation twins are also observed.

NG_{18} at concentrations of H_1, H_2, and H_3 lose most of their stress-bearing ability within 40% strain. The H_3 case even fractures at barely 20% strain. From the grain shape change during deformation, we can see that GB-related intergranular deformation modes are more suppressed as H concentration increases. Although dislocations and twins also decrease as the H concentration increases, they are less influenced than the GB-related deformation modes. GB fracture occurs when GBs are substantially weakened by H segregation, while at the same time, deformation twins and dislocations exert a higher stress than the GBs can withstand. In the low H concentration case (H_1), the weakening of GB strength by H segregation is not as severe, so the dislocations have time to move and pile-up; thus, the fracture surfaces are curved and look like a quasi-cleavage fracture surface. In the high H concentration cases (H_2 and H_3), the GBs are so weakened by H segregation that a few dislocations and deformation twins could exert enough stress to fracture the GBs.

12 nm grain model (NG_{12})

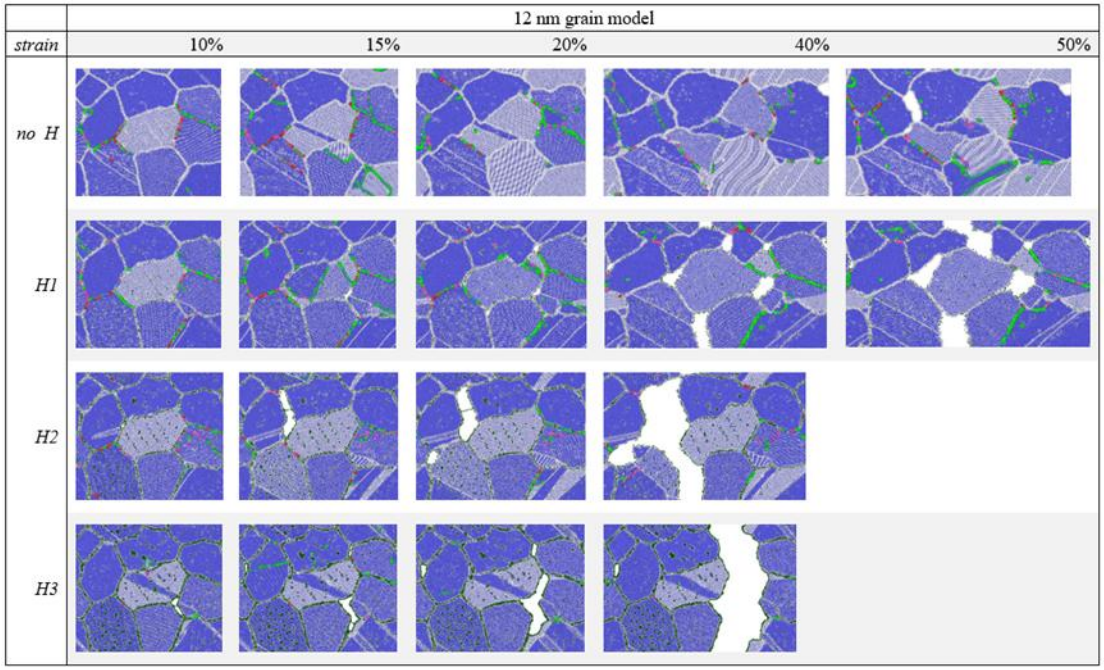

Fig. 7. The snapshots of NG_{12} without H and with H concentrations of H_1, H_2, and H_3 at 10%, 15%, 20%, 40% and 50% uniaxial strain.

The snapshots of NG_{12} during tensile simulations are plotted in Fig. 7. The corresponding stress-strain curves are shown in Fig. 4c. Since 12 nm is higher than the critical grain size for

the inverse Hall-Petch effect, dislocations can nucleate and pile-up in the grain during deformation. In addition to dislocation activities, deformation twins, GB sliding, GB migration and grain rotation are commonly observed in NG_{12} with no H added. Due to the small grain size, GB-related deformation is more important in NG_{12} than that in NG_{18} and NG_{24}.

As the H concentration increases, the observations of dislocations and deformation twins decrease, GBs are mostly pinned to their original positions, and grain rotation occurs much less frequently than that for the no H case. Since GB-related deformation modes, like GB migration and grain rotation, play important roles during plastic deformation of NG_{12}, the suppression of GB-related deformation due to H segregation at the GBs forces NG_{12} to deform by dislocation activities and deformation twins, which can induce GB fracture. Therefore, H segregation to the GBs not only weakens GB cohesive strength but also suppresses GB-related deformation.

6 nm grain model (NG_6)

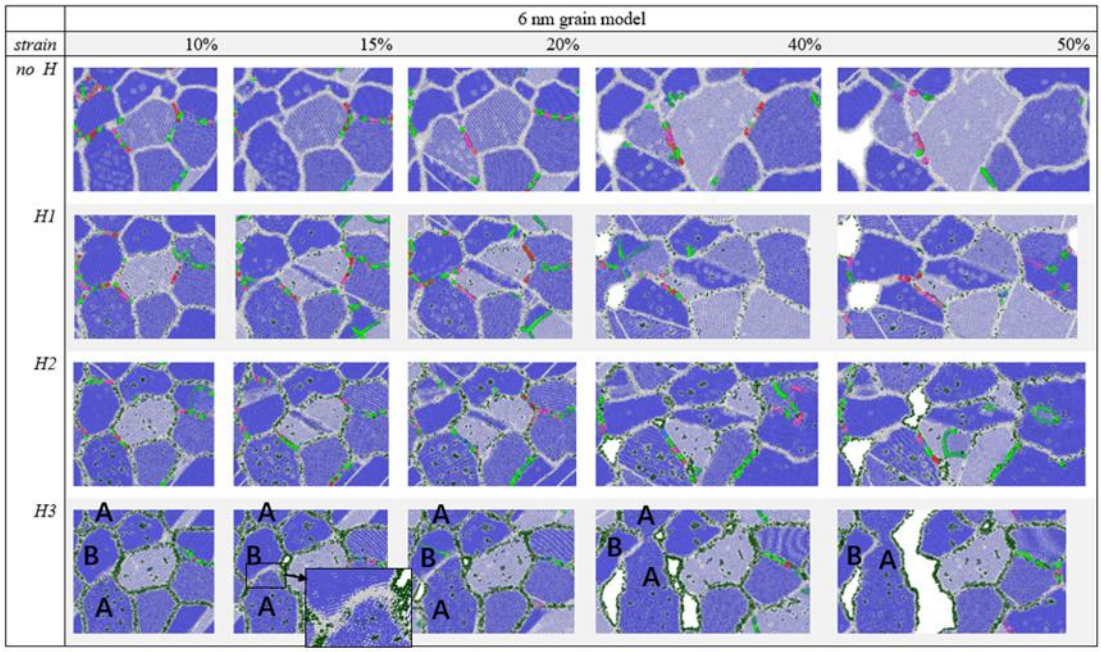

Fig. 8. The snapshots of NG_6 without H and with H concentrations of H_1, H_2, and H_3 at 10%, 15%, 20%, 40% and 50% uniaxial strain.

The snapshots of NG_6 during the tensile simulations are plotted in Fig. 8. The corresponding stress-strain curves are shown in Fig. 4d. In Fig. 8, we can see that similar to NG_{12}, the H atoms segregated at the GBs greatly inhibit the GB-related intergranular deformation modes. As the H concentration increases, the grains retain an increased amount of their original shapes, while grain growth and rotation decrease. Deformation twin and dislocation nucleation are also suppressed by the increased H concentration, as few deformation twins and dislocation activities are observed during the deformation process as the H concentration increases. From the dislocation lines along the GBs, we can see that H segregation largely changes the local atomic configurations and causes a decrease in the density of the GB dislocations. This local atomic configuration change may have resulted in the suppression of GB dislocation nucleation. As deformation twins are also formed by partial dislocation slip, the suppression of dislocation nucleation should also suppress twin formation. This hypothesis can be partly confirmed by Fig. 4d, in which the peak stress of H_3 is higher than those of the other cases, indicating that the onset of plastic deformation, such as full or partial dislocation nucleation, is delayed due to the high H concentration at the GBs. However, despite the inhibiting effect of the H segregation, GB migration is still observed. The GB between grain A and B migrates upwards regardless of the segregated H atoms, leaving the H atoms behind, which can be seen from the enlarged plot of the GB between grain A and B. The H atoms that are originally segregated at the GB between grain A and B move to neighboring boundaries. The GB migration finally results in the growth of grain A.

Compared with models of larger grain size, NG_6 is the least susceptible to HE. The fracture surfaces of NG_6 at H_3 are mostly curved, and the model does not fracture until 47% strain is reached, which is in clear contrast with the flat fracture surfaces in NG_{12}, NG_{18} and NG_{24} at H_3. Due to this obvious difference, we propose two explanations. First, the increased GB density in the 6 nm grain model makes it more likely to deform by GB-related intergranular deformation. Although the intergranular deformation is inhibited by the H segregation at the GBs, some GBs could still migrate and cause grain rotation or grain growth to accommodate the stress (see grain A and B in NG_6-H_3). Second, the increased GB density

in the 6 nm grain model decreases the H concentration per unit length of GB, given that the total H concentrations in the models are the same. As shown in Table. 1, the H_{GB} of NG_6 is less than half of the H_{GB} of NG_{24}, despite the fact that the GB segregation ratio of NG_6 is higher than that of NG_{24} by 65%. The decreased H concentration mitigates the embrittling effect of H segregation, enabling the model to have an increased toughness.

From the above simulation results and analysis, we can conclude that H atoms can suppress GB-related intergranular deformation. The inhibitory effect of H on GB movement can be understood through the impurity-drag theory[59-60], which suggests that solute atoms can greatly decrease GB mobility. The MD simulation performed by Yi et al. [61] also showed that H atoms could hinder GB migration by increasing GB disorder. In addition to GB migration, we suggest that H atoms might also inhibit the nucleation of GB dislocations by changing the local atomic configuration of the GBs. The suppression of plastic deformation induced by H segregation at the GBs along with H-induced weakening of the GB strength cause the early fracture of NG_6-H_3. We can also see that even with high concentration of H along the GBs, NG_6 still retained a high toughness, indicating its high resistance to HE.

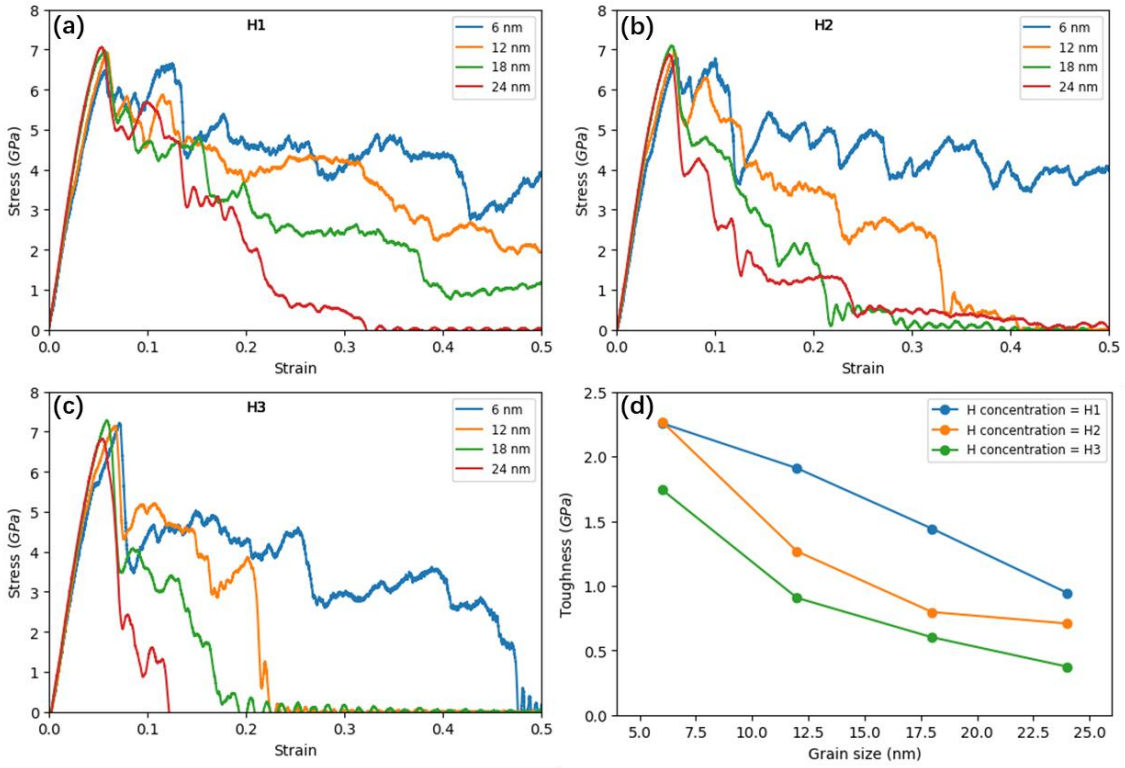

Fig. 9. Stress-strain curves of NG_{24}, NG_{18}, NG_{12}, and NG_6 at different H concentrations. The results are shown for (a) H_1, (b) H_2, and (c) H_3. (d) Toughness versus grain size for NG_{24}, NG_{18}, NG_{12}, and NG_6 with H concentrations of H_1, H_2, and H_3.

Finally, the stress-strain curves of the 4 models at different H concentrations are replotted in Fig. 9 with results of the same H concentrations shown in the same plot. The toughness of the models was calculated by integrating the stress-strain curves, and the toughness versus grain size relations are plotted in Fig. 9d. It should be noted that as NG_6 did not fracture at H_1 and H_2, the toughness calculated is lower than the actual value. For all H concentrations, the toughness values of the models increase as the grain size decreases, confirming the hypothesis that refining the grain size can enhance the HE resistance of nanograined Fe. When the grain size is as small as 6 nm, HE-induced fracture does not happen until the H concentration increases to 3% (H_3). The increased resistance to HE comes not only from the decreased H concentration at the GBs due to the increased GB density in small-grain models but also from the enhanced GB-related intergranular deformation modes due to a reduced grain size.

5. Discussion

Fig. 10 plots the peak stress of the stress-strain curves (Fig. 2d) from the 8 nanograined models versus their grain size and the toughness of the H-segregated models at H_2. The critical grain size d_c is where the transition from the normal Hall-Petch relation to inverse Hall-Petch happens. As the grain size decreases below d_c, the dominant deformation modes transfer from dislocation activities in the grain interiors to GB-related deformation, including GB migration, GB sliding, grain rotation, grain growth, deformation twins and dislocations that are nucleated at the GBs, as shown in Fig. 2b and 2c. In the inverse Hall-Petch region, the GB-segregated H atoms embrittle the NGs by inhibiting GB motion, which increases the difficulty of plastic deformation. However, due to the high density of GBs and abundance of GB-related deformation modes, the small-grain model has a high resistance to HE. In the normal Hall-Petch region, GBs generally play a minor role during plastic deformation, while dislocation activities in the grain interiors become increasingly important as the grain size increases. Hydrogen then influences the toughness by the commonly known

‘hydrogen-enhanced-plasticity-mediated decohesion’ mechanism, where dislocations enhanced by hydrogen pile-up at and impinge GBs to cause the fracture of the already weakened GBs.

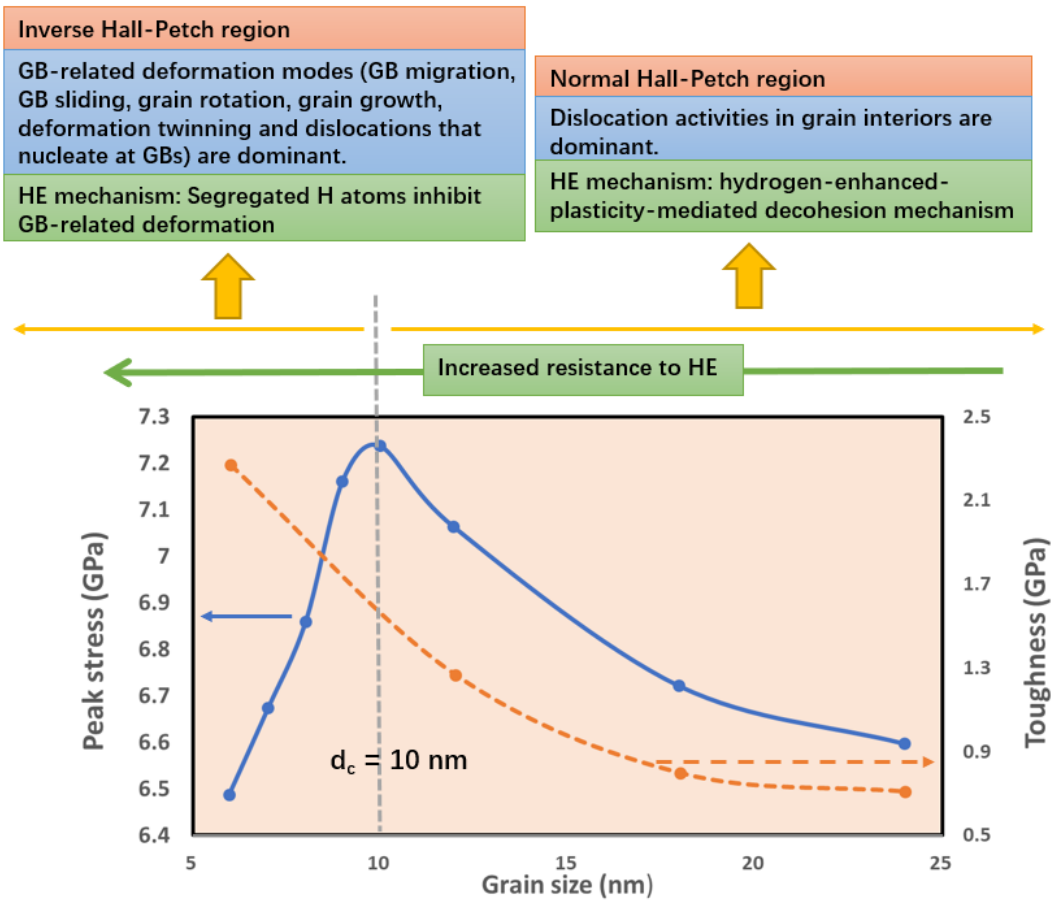

Fig. 10. Peak stress of the stress-strain curves (Fig. 2d) of the 8 nanograined models versus their grain size and toughness versus grain size for NG_{24}, NG_{18}, NG_{12}, and NG_6 with H concentrations of H_2; The critical grain size d_c is where the transition from the normal Hall-Petch relation to inverse Hall-Petch happens.

From the GB segregation results in Table 1, we can see that although the H segregation ratios in the small-grain models are much higher than those in the large-grain models, the H_{GB} values of the small-grain models are still lower than those of the large-grain models, given that the total H concentration is the same. This is due to the high GB density in small-grain models, which has a 'dilution effect' on the H segregation at the GBs. Several studies about the grain-size effect on the HE of nanograined metals have suggested that the 'dilution effect' resulting from a high density of GBs can enhance the HE resistance of materials[36, 38]. However, confirming this hypothesis with experiments is not easy. Here we use MD simulations to provide evidence for the 'dilution effect' from the GBs.

The simulation results confirmed the possibility of increasing HE resistance by grain

refinement to nanosized grains. Grain refinement could have two effects: it may dilute the H concentration at GBs to reduce the H-induced GB decohesion and it may promote GB-related intergranular deformation. In our simulations, the largest grain diameter was only 4 times larger than the smallest; therefore, the 'dilution effect' was not obvious. If we can achieve grain refinement from the micrometer scale to the ~10 nm scale, the GB density would be increased by 10^4 times, and the 'dilution effect' would be much more influential.

Last, we would like to discuss the limitation of the current simulations. First, tensile test simulations were carried out at room temperature and a high strain rate. In real cases, HE usually happens at a low strain rate where the H atoms have enough time to diffuse toward defect sites that are generated during the deformation. However, in our simulation, H atoms do not have enough time to diffuse toward the generated defect sites, making the observed deformation process different from the real case. Therefore, understanding the simulation results should focus on the H segregation effect on GB-related intergranular deformation and the grain-size effect on the plastic deformation mode. Second, the largest grain size simulated is only 24 nm, which is still extremely small. From our simulations, it is difficult to predict the deformation modes and HE mechanism in nanograined materials with grain sizes of approximately 100 nm. At the same time, there are only 9 grains in our models. To obtain a more realistic simulation, one should adopt models with larger grain sizes and more grains than those that were used herein, which is planned for our following studies. However, the current study focuses on the comparative analysis of the HE mechanism in models with different grain sizes. We believe that from the simulation results, it is possible to reveal the grain-size effect on the plastic deformation and the HE mechanism of nanograined Fe. Apart from the above two limitations, it should be noted that the results and discussions of the current research are based on the assumption that the H concentrations in models with different grain sizes are the same. Considering that GBs are effective hydrogen traps, in real cases the H concentration in smaller-grain samples would be higher than their coarser-grain counterparts. A more realist model should consider the different hydrogen uptake in models with different GB density. Such kind of data could only come from experimental results and

would be our next step.

Conclusions

In summary, we performed a series of MD simulations to investigate the grain-size effect on the HE mechanism in nanograined Fe. Models of different grain sizes but with the same grain distribution were built. The equilibrium atomic structures of the models without H and with H segregation were obtained by heating and cooling process. The H segregation results show that given the same total H concentration, the segregation ratio increases with decreasing grain size; however, in contrast, the H concentration values at GBs decrease with decreasing grain size, owing to the high GB density in the small-grain models. The HE mechanism in models with different grain sizes is revealed by uniaxial tensile test simulations. It is found that in the large-grain models (NG_{18} and NG_{24}), dislocation activities are the main deformation modes. Therefore, for the models with large grains, the HE mechanism involves the interaction of dislocations, GBs and H atoms that segregate at GBs, and the HE mechanism could be well described by the 'hydrogen-enhanced-plasticity-mediated decohesion mechanism[29, 33]; however, in the small-grain models, GB-related intergranular deformation, including GB migration, GB sliding, grain rotation, grain growth, deformation twins and dislocations that nucleate at GBs dominate the plastic deformation. The segregated H is then found to mainly influence the toughness of the models by inhibiting GB-related deformation. By comparing the mechanical response of models with different grain sizes and the same total hydrogen concentration, we can see that the small-grain model has an increased HE resistance, not only because the high GB density dilutes the H concentration at the GBs but also because of the abundant GB-related deformation modes.

Acknowledgments

The present research was conducted at Shenzhen University. We would like to thank the funding support from the Chinese National Natural Science Foundation (51778370, 51538007), Natural Science Foundation of Guangdong (2017B030311004) and the Shenzhen science and technology project (JCYJ20170818094820689)

References

1. Li, W. L.; Tao, N. R.; Lu, K., Fabrication of a gradient nano-micro-structured surface layer on bulk copper by means of a surface mechanical grinding treatment. *Scripta Materialia* **2008,** *59* (5), 546-549.
2. Lu, S.; Wang, Z.; Lu, K., Strain-induced Microstructure Refinement in a Tool Steel Subjected to Surface Mechanical Attrition Treatment. *Journal of Materials Science & Technology* **2010,** *26* (3), 258-263.
3. Tao, N. R.; Wang, Z. B.; Tong, W. P.; Sui, M. L.; Lu, J.; Lu, K., An investigation of surface nanocrystallization mechanism in Fe induced by surface mechanical attrition treatment. *Acta Materialia* **2002,** *50* (18), 4603-4616.
4. Lu, K.; Lu, J., Nanostructured surface layer on metallic materials induced by surface mechanical attrition treatment. *Materials Science and Engineering: A* **2004,** *375-377*, 38-45.
5. Nieman, G. W.; Weertman, J. R.; Siegel, R. W., Microhardness of nanocrystalline palladium and copper produced by inert-gas condensation. *Scripta Metallurgica* **1989,** *23* (12), 2013-2018.
6. Ullal, Y.; Hegde, A. C., Electrodeposition and electro-catalytic study of nanocrystalline Ni–Fe alloy. *International Journal of Hydrogen Energy* **2014,** *39* (20), 10485-10492.
7. Du, C.; Jin, S.; Fang, Y.; Li, J.; Hu, S.; Yang, T.; Zhang, Y.; Huang, J.; Sha, G.; Wang, Y.; Shang, Z.; Zhang, X.; Sun, B.; Xin, S.; Shen, T., Ultrastrong nanocrystalline steel with exceptional thermal stability and radiation tolerance. *Nature Communications* **2018,** *9* (1), 5389.
8. Borovikov, V.; Mendelev, M. I.; King, A. H., Effects of solutes on dislocation nucleation from grain boundaries. *International Journal of Plasticity* **2017,** *90*, 146-155.
9. Wu, X. L.; Liao, X. Z.; Srinivasan, S. G.; Zhou, F.; Lavernia, E. J.; Valiev, R. Z.; Zhu, Y. T., New Deformation Twinning Mechanism Generates Zero Macroscopic Strain in Nanocrystalline Metals. *Physical Review Letters* **2008,** *100* (9), 095701.
10. Kobler, A.; Lohmiller, J.; Schäfer, J.; Kerber, M.; Castrup, A.; Kashiwar, A.; Gruber, P. A.; Albe, K.; Hahn, H.; Kübel, C., Deformation-induced grain growth and twinning in nanocrystalline palladium thin films. *Beilstein J Nanotechnol* **2013,** *4*, 554-566.
11. Luo, X.-M.; Zhu, X.-F.; Zhang, G.-P., Nanotwin-assisted grain growth in nanocrystalline gold films under cyclic loading. *Nature Communications* **2014,** *5*, 3021.
12. Shan, Z.; Stach, E. A.; Wiezorek, J. M. K.; Knapp, J. A.; Follstaedt, D. M.; Mao, S. X., Grain Boundary-Mediated Plasticity in Nanocrystalline Nickel. *Science* **2004,** *305* (5684), 654.
13. Schiøtz, J.; Di Tolla, F. D.; Jacobsen, K. W., Softening of nanocrystalline metals at very small grain sizes. *Nature* **1998,** *391* (6667), 561-563.
14. Hirth, J. P., Effects of hydrogen on the properties of iron and steel. *Metallurgical*

Transactions A **1980,** *11* (6), 861-890.
15. Louthan, M. R.; Caskey, G. R., Hydrogen transport and embrittlement in structural metals. *International Journal of Hydrogen Energy* **1976,** *1* (3), 291-305.
16. El kebir, O. A.; Szummer, A., Comparison of hydrogen embrittlement of stainless steels and nickel-base alloys. *International Journal of Hydrogen Energy* **2002,** *27* (7), 793-800.
17. Liu, Y. L.; Zhang, Y.; Zhou, H. B.; Lu, G. H., Vacancy trapping mechanism for hydrogen bubble formation in metal. *Physical Review B Condensed Matter & Materials Physics* **2009,** *79* (17), 172103.
18. Nagumo, M.; Takai, K., The predominant role of strain-induced vacancies in hydrogen embrittlement of steels: Overview. *Acta Materialia* **2019,** *165*, 722-733.
19. Martin, M. L.; Dadfarnia, M.; Nagao, A.; Wang, S.; Sofronis, P., Enumeration of the hydrogen-enhanced localized plasticity mechanism for hydrogen embrittlement in structural materials. *Acta Materialia* **2019,** *165*, 734-750.
20. Koyama, M.; Rohwerder, M.; Cem Tasan, C.; Bashir, A.; Akiyama, E.; Takai, K.; Raabe, D.; Tsuzaki, K., *Recent progress in microstructural hydrogen mapping in steels: quantification, kinetic analysis, and multi-scale characterisation*. 2017.
21. Koyama, M.; Yamasaki, D.; Nagashima, T.; Tasan, C. C.; Tsuzaki, K., In situ observations of silver-decoration evolution under hydrogen permeation: Effects of grain boundary misorientation on hydrogen flux in pure iron. *Scripta Materialia* **2017,** *129*, 48-51.
22. Takai, K.; Seki, J.; rsquo; ichi; Homma, Y., Observation of Trapping Sites of Hydrogen and Deuterium in High-Strength Steels by Using Secondary Ion Mass Spectrometry. *Materials Transactions, JIM* **1995,** *36* (9), 1134-1139.
23. Peral, L. B.; Zafra, A.; Belzunce, J.; Rodríguez, C., Effects of hydrogen on the fracture toughness of CrMo and CrMoV steels quenched and tempered at different temperatures. *International Journal of Hydrogen Energy* **2019,** *44* (7), 3953-3965.
24. Wang, S.; Martin, M. L.; Sofronis, P.; Ohnuki, S.; Hashimoto, N.; Robertson, I. M., Hydrogen-induced intergranular failure of iron. *Acta Materialia* **2014,** *69*, 275-282.
25. Liu, Q.; Zhou, Q.; Venezuela, J.; Zhang, M.; Atrens, A., Hydrogen influence on some advanced high-strength steels. *Corrosion Science* **2017,** *125*, 114-138.
26. Ogawa, Y.; Birenis, D.; Matsunaga, H.; Takakuwa, O.; Yamabe, J.; Prytz, Ø.; Thøgersen, A., The role of intergranular fracture on hydrogen-assisted fatigue crack propagation in pure iron at a low stress intensity range. *Materials Science and Engineering: A* **2018,** *733*, 316-328.
27. Zafra, A.; Peral, L. B.; Belzunce, J.; Rodríguez, C., Effect of hydrogen on the tensile properties of 42CrMo4 steel quenched and tempered at different temperatures. *International Journal of Hydrogen Energy* **2018,** *43* (18), 9068-9082.
28. Novak, P.; Yuan, R.; Somerday, B. P.; Sofronis, P.; Ritchie, R. O., A statistical, physical-based, micro-mechanical model of hydrogen-induced intergranular fracture in steel. *Journal of the Mechanics and Physics of Solids* **2010,** *58* (2), 206-226.

29. Wan, L.; Geng, W. T.; Ishii, A.; Du, J.-P.; Mei, Q.; Ishikawa, N.; Kimizuka, H.; Ogata, S., Hydrogen embrittlement controlled by reaction of dislocation with grain boundary in alpha-iron. *International Journal of Plasticity* **2019,** *112*, 206-219.
30. Tehranchi, A.; Curtin, W. A., Atomistic study of hydrogen embrittlement of grain boundaries in nickel: II. Decohesion. *Modelling and Simulation in Materials Science and Engineering* **2017,** *25* (7), 075013.
31. Huang, S.; Chen, D.; Song, J.; McDowell, D. L.; Zhu, T., Hydrogen embrittlement of grain boundaries in nickel: an atomistic study. *npj Computational Materials* **2017,** *3* (1), 28.
32. Wang, S.; Martin, M. L.; Robertson, I. M.; Sofronis, P., Effect of hydrogen environment on the separation of Fe grain boundaries. *Acta Materialia* **2016,** *107*, 279-288.
33. Nagao, A.; Dadfarnia, M.; Somerday, B. P.; Sofronis, P.; Ritchie, R. O., Hydrogen-enhanced-plasticity mediated decohesion for hydrogen-induced intergranular and "quasi-cleavage" fracture of lath martensitic steels. *Journal of the Mechanics and Physics of Solids* **2018,** *112*, 403-430.
34. Mine, Y.; Matsumoto, S.; Horita, Z., Strengthening and hydrogen embrittlement of ultrafine-grained Fe–0.01mass% C alloy processed by high-pressure torsion. *Corrosion Science* **2011,** *53* (9), 2969-2977.
35. Mine, Y.; Horita, N.; Horita, Z.; Takashima, K., Effect of ultrafine grain refinement on hydrogen embrittlement of metastable austenitic stainless steel. *International Journal of Hydrogen Energy* **2017,** *42* (22), 15415-15425.
36. Bai, Y.; Momotani, Y.; Chen, M. C.; Shibata, A.; Tsuji, N., Effect of grain refinement on hydrogen embrittlement behaviors of high-Mn TWIP steel. *Materials Science and Engineering: A* **2016,** *651*, 935-944.
37. Fan, Y. H.; Cui, F.; Lu, L.; Zhang, B., A nanotwinned austenite stainless steel with high hydrogen embrittlement resistance. *Journal of Alloys and Compounds* **2019,** *788*, 1066-1075.
38. Zan, N.; Ding, H.; Guo, X.; Tang, Z.; Bleck, W., Effects of grain size on hydrogen embrittlement in a Fe-22Mn-0.6C TWIP steel. *International Journal of Hydrogen Energy* **2015,** *40* (33), 10687-10696.
39. Chen, S.; Zhao, M.; Rong, L., Effect of grain size on the hydrogen embrittlement sensitivity of a precipitation strengthened Fe–Ni based alloy. *Materials Science and Engineering: A* **2014,** *594*, 98-102.
40. Song, J.; Curtin, W., Atomic mechanism and prediction of hydrogen embrittlement in iron. *Nature materials* **2013,** *12* (2), 145.
41. Zhou, X.; Ouyang, B.; Curtin, W. A.; Song, J., Atomistic investigation of the influence of hydrogen on dislocation nucleation during nanoindentation in Ni and Pd. *Acta Materialia* **2016,** *116*, 364-369.
42. Tehranchi, A.; Curtin, W. A., Atomistic study of hydrogen embrittlement of grain boundaries in nickel: I. Fracture. *Journal of the Mechanics and Physics of Solids* **2017,** *101*, 150-165.

43. Xing, X.; Chen, W.; Zhang, H., Atomistic study of hydrogen embrittlement during cyclic loading: Quantitative model of hydrogen accumulation effects. *International Journal of Hydrogen Energy* **2017,** *42* (7), 4571-4578.
44. Xing, X.; Yu, M.; Chen, W.; Zhang, H., Atomistic simulation of hydrogen-assisted ductile-to-brittle transition in α-iron. *Computational Materials Science* **2017,** *127*, 211-221.
45. Barrows, W.; Dingreville, R.; Spearot, D., Traction–separation relationships for hydrogen induced grain boundary embrittlement in nickel via molecular dynamics simulations. *Materials Science and Engineering: A* **2016,** *650*, 354-364.
46. Farkas, D.; Van Swygenhoven, H.; Derlet, P. M., Intergranular fracture in nanocrystalline metals. *Physical Review B* **2002,** *66* (6), 060101.
47. Latapie, A.; Farkas, D., Molecular dynamics investigation of the fracture behavior of nanocrystalline α-Fe. *Physical Review B* **2004,** *69* (13), 134110.
48. Schiøtz, J., Atomic-scale modeling of plastic deformation of nanocrystalline copper. *Scripta Materialia* **2004,** *51* (8), 837-841.
49. Shimokawa, T.; Nakatani, A.; Kitagawa, H., Grain-size dependence of the relationship between intergranular and intragranular deformation of nanocrystalline Al by molecular dynamics simulations. *Physical Review B* **2005,** *71* (22), 224110.
50. Van Swygenhoven, H.; Derlet, P. M.; Frøseth, A. G., Nucleation and propagation of dislocations in nanocrystalline fcc metals. *Acta Materialia* **2006,** *54* (7), 1975-1983.
51. Zhang, Y.; Millett, P. C.; Tonks, M.; Biner, S. B., Deformation twins in nanocrystalline body-centered cubic Mo as predicted by molecular dynamics simulations. *Acta Materialia* **2012,** *60* (18), 6421-6428.
52. Zhu, Y.; Li, Z.; Huang, M., Solute hydrogen effects on plastic deformation mechanisms of α-Fe with twist grain boundary. *International Journal of Hydrogen Energy* **2018,** *43* (22), 10481-10495.
53. Li, S.; Li, Y.; Lo, Y.-C.; Neeraj, T.; Srinivasan, R.; Ding, X.; Sun, J.; Qi, L.; Gumbsch, P.; Li, J., The interaction of dislocations and hydrogen-vacancy complexes and its importance for deformation-induced proto nano-voids formation in α-Fe. *International Journal of Plasticity* **2015,** *74*, 175-191.
54. Zhu, Y.; Li, Z.; Huang, M.; Fan, H., Study on interactions of an edge dislocation with vacancy-H complex by atomistic modelling. *International Journal of Plasticity* **2017,** *92*, 31-44.
55. Steve, P., *Fast parallel algorithms for short-range molecular dynamic*. Academic Press Professional, Inc.: 1995; p 1-19.
56. Stukowski, A., Visualization and analysis of atomistic simulation data with OVITO-the Open Visualization Tool. *Modelling & Simulation in Materials Science & Engineering* **2010,** *18* (6), 2154-2162.
57. Honeycutt, J. D.; Andersen, H. C., Molecular dynamics study of melting and freezing of small Lennard-Jones clusters. *The Journal of Physical Chemistry* **1987,** *91*

(19), 4950-4963.
58. Zhang, Y.; Millett, P. C.; Tonks, M.; Biner, B., Deformation-twin-induced grain boundary failure. *Scripta Materialia* **2012,** *66* (2), 117-120.
59. Cahn, J. W., The impurity-drag effect in grain boundary motion. *Acta Metallurgica* **1962,** *10* (9), 789-798.
60. Vilenkin, A., Interaction of Solute Impurity with Grain Boundary: The Impurity Drag Effect. *Interface Science* **2001,** *9* (3-4), 323-329.
61. Yu, Y.; Shu, X.; Liu, Y.; Niu, L.-L.; Jin, S.; Gao, F.; Lu, G., Effect of hydrogen on grain boundary migration in tungsten. *Science China Physics, Mechanics & Astronomy* **2015,** *58*.